https://doi.org/10.1016/j.jlumin.2019.03.043

Fabrication of Luminescent PtS_2 Quantum Dots

Xinyu Wang[a,b], Hui Long[a,b], Wayesh Qarony[a,b], Chun Yin Tang[a,b], Huiyu Yuan[a,b], Yuen Hong Tsang[a,b]*

[a] *The Hong Kong Polytechnic University Shenzhen Research Institute, Shenzhen, Guangdong, China.*

[b] *Department of Applied Physics and Materials Research Centre, The Hong Kong Polytechnic University, Hung Hom, Kowloon, Hong Kong, China.*

*Corresponding author: yuen.tsang@polyu.edu.hk

Abstract

Platinum disulfide (PtS_2), a member of the recently developed group 10 transition metal dichalcogenide (TMD) materials, exhibits great potential in optoelectronics applications. Nevertheless, its photoluminescence (PL) behaviour still remains obscure. Quantum dots (QDs) are believed having the capability to enhance photoluminescence property compared to the bulky or layered structure owing to their quantum confinement effects. Inspired by remarkable PL enhancement works on other TMD materials QDs, the fabrication of PtS_2 QDs suspension via a low-cost liquid exfoliation technique is demonstrated in this work. The PtS_2 QDs with an average diameter of 3.9 nm and average thickness of 2.9 nm are observed, respectively. For the first time, the PL spectra of PtS_2 QDs suspension are successfully obtained and monitored over time. The PL spectra display an excitation-dependent luminescence. The maximum emission peak is observed at 407.2 nm for the excitation wavelength of 330 nm. This PtS_2 QDs also shows a decent long-term stability. These results open up encouraging prospects of luminescence applications of PtS_2 QDs.

Keywords: Optical materials and properties; Luminescence; PtS_2; Quantum dots

1. Introduction

In the past decade, layered materials have gained considerable attention in the optoelectronics materials and devices [1-3]. The optical and electrical properties of layered materials can be tailored by precisely controlling

the size and dimension according to the applications needs, which could as a consequence significantly enhance the performance along with the expansion of their applications. Due to the excellent electrical properties and low Johnson noise of Graphene after scaling down from bulk graphite to two-dimensional (2D) structure, it has become a competitive candidate for the channel of field effect transistor [1]. Similar to graphene, layered transition metal dichalcogenide (TMD) materials such as MoS_2 or WS_2 outperform in a wide range of applications including but not limited to catalysis, energy storage, electronics devices, and bio-pharmacy [2–4]. Unlike the conventional transition metal sulfides such as PbS or CdS, TMD materials are arranged in 2D layered structures and their bandgaps exhibit layer-dependent property [3]. Many of the research efforts are focused on the optimization of the fabrication process of low dimension of these layered nanomaterials as it benefits in a wide range of research fields ranging from material science to the novel device applications [3,5].

Quantum dot (QD) was explored by further reducing dimensions of 2D layered materials to ideally zero dimension. This novel structure of material exhibits strong quantum confinement and boundary effect leading to unique and excellent electrical or optical properties that exceed its few- or mono-layer counterpart [6]. For instance, carbon QDs, generally defined as carbon that smaller than twice the size of its exciton Bohr radius, resulting in quantum confinement, exhibits distinguished optical properties of tunable fluorescence emissions and up-conversion fluorescence compared to the bulky graphite or graphene sheet [7]. The QDs materials also exhibit larger transition energy in comparison to the layer structure due to quantum confinement effects that are capable to obtain enhanced photoluminescence (PL) in certain spectra [6-9]. QDs have played prominent roles for a wide range of novel applications including non-linear optics [10,11], photo-catalysis [12,13], photovoltaics [14], and bio-imaging [15]. The fabrication of quantum dots with the novel 2D materials is currently considered to be a crucial and demanding research field due to exclusive characteristics and wide applied areas.

Recently, layered group 10 TMD materials of Platinum disulfide (PtS_2) and Platinum diselenide ($PtSe_2$) have gained significant attention owing to their promising electronic and optical properties. In a typical octahedral unit cell structure of group 10 TMD material, one transition metal atom is surrounded by 6 chalcogen atoms [16, 17]. According to the density functional theory (DFT) calculation, PtS_2 possesses an indirect band gap with layer-dependent nature. As the thickness decreases from bulk structure to mono-layer, the band gap energy

of such material varies from 0.25 eV to 1.6 eV, indicating an optical spectrum ranging from visible to infrared wavelength [17]. Under the ambient temperature, PtS_2 also exhibits a considerable electrical conductivity of 1107 $cm^2 V^{-1} s^{-1}$, which is comparable to that of black phosphorus [18, 19]. Remarkable research progress has been achieved so far on the applications of PtS_2 based field-effect transistor (FET) [16], pulsed laser generation [20], and hydrogen evolution reaction (HER) [21]. However, it has been reported that the PL signals exhibited by PtS_2 at a scale from bulk to monolayer are too weak to be detected [17]. This statement aroused our interest to further investigate its PL behaviors.

Quantum dots are reported to exhibit larger transition energy in comparison to the layer structure due to quantum confinement effects that are capable to obtain enhanced PL in certain spectra [6, 8, 9]. Inspired by quantum confinement effect, the current study is focused on the fabrication of PtS_2 QDs suspension to enhance its PL performance and obtain the emission spectra. Expensive techniques such as Chemical vapor transport (CVT) [16, 17] and molecular beam epitaxy (MBE) [22, 23] are generally utilized to produce few-layer group 10 TMD materials. The synthesize methods and characteristics of PtS_2 QDs are rarely reported so far. In this work, PtS_2 QDs suspension is successfully obtained by a low-cost liquid exfoliation method. The emission spectra of PtS_2 QDs are successfully confirmed and firstly demonstrated in this work. The characterizations of PtS_2 QDs and their PL behaviors reveal the potentiality of this material in the field of luminescence related applications such as imaging, light-emitting diode, or bio-sensor.

2. Experimental Section

2.1 Materials Fabrication

PtS_2 QDs suspension was fabricated by high intensity ultrasonic liquid exfoliation followed by dialysis shown in Fig. 1. The 50 mg bulk PtS_2 powder (Alfa Aesar) was added into 250 ml of deionized (DI) water. Then the probe sonication (SCIENTZ-1200E, Ningbo Scientz Biotechnology Co., Ltd.) was conducted to the mixture under the power of 1200 W with 20 kHz below 27 ℃ for 12 hours, while an ultrasound probe time of 2 s at an interval of 4 s was maintained. Afterwards, a sonication bath with 40 kHz for 6h was applied to the mixture and followed by centrifuging at 8000 rpm for 20 min to eliminate unexfoliated bulky PtS_2. The collected supernatant

liquor was subjected to dialysis using a dialysis membrane (cut-off 3.5 kDa) for 24 h. The solution outside the dialysis membrane was taken as the PtS_2 QDs solution kept in ambient environment for several days, 3 months, and 6 months.

2.2 Characterizations

The PL emission spectra of as-prepared PtS_2 QDs solution were recorded using Edinburgh CD920 on excitation at given wavelength. The measurement is conducted under room temperature by using Xenon lamp as excitation source. UV-Vis absorption spectroscopy was conducted by Shimadzu UV-2550. The PtS_2 QDs solution was contained in quartz cuvettes for PL and UV-Vis characterizations. The morphology and lattice fringes were observed by Scanning Transmission Electron Microscopy (STEM, Jeol JEM-2100F). The height information of PtS_2 QDs was measured by Atomic Force Microscopy (Bruker Nanoscope 8). The AFM sample was prepared by spin-coating the solution on the surface of quartz substrate followed by drying in the ambient laboratory condition. X-ray photoelectron spectroscopy (XPS, ESCALAB 250Xi, Thermo Fisher Scientific) was carried out to reveal the chemical composition with achromatic 200W Al Kα as the X-ray source and the resolution of 0.10 eV. The powder of the raw material was kept in the oven with 60 °C for 3 h for drying before conducting the XPS characterization.

3. Results and Discussion

In this work, PtS_2 QDs were fabricated by conducting ultrasonic exfoliation in DI water. The electrical energy in the equipment was firstly converted to mechanical energy via piezoelectric effect. When sonication probe introduces, an intense mechanical vibration is generated in liquid. As a consequence of that an acoustic energy is generated in the form of ultrasonic waves. The ultrasonic waves are strong enough to oscillate the liquid, resulting in the circulation of low and high pressure in DI water. In the period of rarefaction, many vacuum bubbles are generated within the mixture of DI water and PtS_2 powder attributing to the increase of molecular distance. When the rarefaction alternates with compression, those bubbles are intensely collapsed. Localized high temperature, high pressure and wild flow of liquid are induced accompanied by the implosion. This so called cavitation process offers massive kinetic energy to overcome Van der Waals force for decomposing and grinding the PtS_2 bulk powder into smaller particles and quantum dots counterpart [24,25].

The PtS_2 QDs are observed by Scanning transmission electron microscopy (STEM) as shown in Fig. 2. The as-prepared PtS_2 QDs and the statistics of size distribution are depicted in Fig. 2(a) and 2(c) demonstrating an average diameter of 3.9 nm obtained by measuring 44 QDs. Fig. 2(b) captured by a high-resolution of TEM shows the crystalline characteristic of a typical as-prepared QD with a diameter of 3.74 nm. The sharp lattice fringe with a 0.29 nm of interplanar spacing corresponding to the (001) planes of PtS_2 [16, 17], indicating its single crystalline nature. After 3 months storage under ambient conditions, PtS_2 QDs remained the well-dispersive status in DI water as the TEM images shown in Fig. 2(d) and 2(e). The average diameter among 43 QDs become 4.3 nm, shown in Fig. 2(f), possibly due to PtS_2's poor solubility in water. The significant size increase of PtS_2 nanoparticles was observed after 6 months storage as shown in Fig. 2(g). By magnifying the scale to high resolution, Fig. 2(h) can be obtained displaying several QDs agglomerate into one larger nanoparticle, which is counted as one particle for statistics of size distribution, shown in Fig. 2(i). This increase of size may also because of restacking of the exfoliated nanoparticles to thicker ones by the Van der Waals forces. The average size of 44 nanoparticles is about 10.5 nm.

The as-prepared PtS_2 QDs were found scattering on the quartz substrate sample by conducting AFM measurement. The 1×1 μm^2 image of the substrate surface, the section analysis (inset), and the thickness analysis are presented in Fig. 3. Two sharp signals of PtS_2 QDs can be recognized precisely along the section with height of 4.0 nm and 3.4 nm, respectively, suggesting they consist of 8 and 7 layers [17]. The average thickness of PtS_2 QDs is obtained to be 2.9 nm by measuring 36 QDs. By comprehensive analysis of size characteristics obtained by AFM and TEM, the intense ultrasonic energy is proved to be capable to weaken the Van der Waals force inside the particles and even break them into the form of nanoscale QDs.

The chemical composition in raw material of PtS_2 powder was investigated by XPS measurement, whereas the signal of as-prepared QD sample is too weak to be detected for its insufficient quantity in the solvent. As observed in XPS spectrum in Fig. 4(a) and 4(b), the chalcogen in PtS_2 can be split peaks into 162.9 eV and 164.2 eV, respectively, arising from the S2p1/2 with lower binding energy and S2p3/2 with higher binding energy in spin-orbit splitting. On the surface of the sample, a part of S^{2-} in PtS_2 is transformed to sulphate series. The peak detected in Fig. 4(b) at binding energy of 169.6 eV indicates that the sulphates may exist as forms of

HSO_4^- or SO_4^{2-} [21,26]. These considerable sulphate series might produce compound such as $PtSO_4$, $Pt(HSO_4)_2 \cdot H_2O$ etc., which significantly contribute to the Pt(II), corresponding to Pt4f7/2 and Pt4f5/2 signals at 72.2 eV and 75.5 eV, respectively, on the surface of PtS_2. The predominant Pt(II) rather than Pt(IV) (at binding energy of Pt4f7/2 = 73.1 eV and Pt4f5/2 = 76.5 eV) and the presence of sulphate series illustrate the phenomenon of partial oxidation on the surface of the sample during the drying process. The atomic percentages deduced from XPS test were determined to be 15.01% and 26.05% for Pt4f and S2p, respectively, from the integrated areas of their peaks. The stoichiometric ratio of S2p to Pt4f is less than the expected value of 2. This deviation may attribute to the absence of chalcogens due to yielding the sulphate series by cause of oxidization.

The PL spectra of the PtS_2 QDs samples were measured under various excitation wavelengths. Fig. 5(a) presents the emission spectra of as-prepared PtS_2 QDs sample. The red-shifts of emission peaks ranging from 395.7 nm to 464.4 nm account for increasing excitation wavelength from 300 nm to 390 nm. This excitation-dependent luminescent property has also been reported on various types of QDs such as carbon QDs [27,28], alloying inorganic semiconductor QDs [29,30], and traditional TMDs QDs [8,9]. The mechanism attribute to the size effect on the band gap energies of the QDs. Excited by Xenon arc lamp, the smaller QDs with wider band gap emit at shorter wavelength while the larger QDs with narrow band gap emit at longer wavelength, indicating the poly-dispersity characteristic of this PtS_2 QDs sample. The excitation wavelength versus the peak position of emission is illustrated in Fig. 5(d). This figure explains that the as-prepared QDs suspension exhibits a linear behavior, attributing to the quantum size effect which is schematically explained in Fig. 5(e), that the bandgap energy is dependent on the size of QD. The consistency of emission wavelengths provides the evidence of quantum confinement effect. The observed luminescent intensity keeps increasing during the red-shift of excitation wavelength starting from 300 nm and reaches to the maximum signal of 407.2 nm excited at 330 nm. Photoluminescence excitation (PLE) spectrum for the highest emission peak occurring at 407.2 nm wavelength was depicted in Fig. 6. The excitation peak appearing at 328.5 nm wavelength can be considered as major contributor to 407.2 nm emission wavelength. The UV-Vis spectrum of PtS_2 QDs solution was scanned and included in Fig. 6 as well. The absorbance curve displays an absorption peak at 271.5 nm. The weak absorption trend appears between 311-387 nm might attribute to nanoparticles in larger scales.

This excitation wavelength dependent behavior may also due to various pathways including but not limited to poly-dipersity. Förster resonant energy transfer (FRET), as a result of re-absorption between neighboring QDs, can be responsible for the red-shift of the spectrum [31]. Another scenario would account for the excitation wavelength dependence could be the fickle surface morphology of the quantum dots. After absorption process, the charges will be separated and trapped at surface locations. A recent work reported that the radiative recombination of these charges, governed by radiative rates, differ from various surface structure of quantum dots [32]. The inhomogeneous distribution of absorption spectrum reflected increasing radiative rates and at higher-energy and decreasing radiative rates at lower-energy in Fig. 6, agreeing with the fact in Fig. 5 that the PL emissions intensity increases from shorter wavelength and decreases from a certain wavelength to longer wavelength. The energy transfer in functional groups may also alter the emission spectrum [33]. Since the raw materials is pure PtS_2, and the solvent is DI water, the functional groups are assumed to play a minor role to the influence of emission spectrum in this work.

A 0.73 eV stokes shift is observed for 328.5 nm excitation wavelength and the 407.2 nm emission wavelength. Such large value might due to the quantum confinement effect, which leads to interaction between discrete levels of electron and hole. The spatial overlaps for wave functions of electron and hole increase dramatically when the materials sizes decrease to QD scale [34]. Therefore, the fine structure splitting between the lowest active singlet excitonic states and passive triplet states are much larger than its layer or bulk counterpart [34,35]. Deexcitation, which origins when rapid thermalization takes place from higher active energy states to passive triplet states, results in a red shift of emission spectra. As a consequence, it yields a larger stokes shift. The environment might also take account for the stokes shift. Since water is polar solvent, it can reorient the excited state dipole of quantum dots, which leads to lower energy and red shifts of emission wavelength. This so called solvent relaxation might lead to substantial stokes shifts [36].

As shown in Table 1, the PL Quantum Yield (QY) of PtS_2 QDs was estimated to be 1.28% by comparing the emission peak occurring at 407.21 nm and absorbance of as-prepared sample with the reference 1,8-ANS of known QY (0.0032) [37]. The 1,8-ANS was dissolved in water. Since the solvent of PtS_2 QDs is water as well,

the refractive index of the sample and the reference can be considered to be equal, and the value is 1.33. The QY for the PtS_2 QDs sample can be calculated as Equation 1.

$$\mathrm{QY} = QY_{ref}\frac{\eta^2}{\eta_{ref}^2}\frac{I}{I_{ref}}\frac{A_{ref}}{A} \quad (1)$$

where QY_{ref} is the quantum yield of the reference compound, η is the refractive index of the solution, I is the integrated emission intensity and A is corresponding to the absorbance of the sample and the reference.

Table 1.

Quantum Yield of PtS_2 QDs

Sample	**Integrated emission intensity (I)**	**Absorbance**	**Refractive index of solvent (η)**	**Quantum Yield (QY)**
1,8-ANS	97.2924	0.87011	1.33	0.0032 (known) [27]
PtS_2 QDs	97.9681	0.21925	1.33	0.0128

The long-term PL stability of PtS_2 QDs are monitored at stage of 3 months and 6 months stored under ambient conditions, shown in Fig. 5(b) and 5(c). To illustrate the difference of the emission peak positions of the three samples, emission peak wavelengths are plotted against the excitation wavelengths shown in Fig. 5(d). The emission peak was red shifted significantly from 394.4 nm and 395 nm representing for as-prepared sample and 3 months sample, respectively, to 423.6 nm for 6 months sample under 300 nm of excitation wavelength. The 390 nm of excitation wavelength gives emission peaks at 455.7 nm, 447.3 nm, and 449.7 nm for as-prepared, 3 months, and 6 months sample, respectively. These results indicate 61.3 nm, 52.3 nm, and 26.1 nm emission peak positions shifted for 3 samples mentioned above, respectively, when the excitation wavelength was tuned from 300 nm to 390 nm. The emission peak excited under 300 nm wavelength and smaller range of emission peak shifted for the 6 months sample represent its weaker excitation-dependent property compared with the as-

prepared and 3 months samples. These results agree well with the size of nanoparticle shown in Fig. 2. The strong excitation-dependent property of 3 months sample shows well-dispersive status of QDs in the solution according to the quantum size effect. The weak excitation-dependent property of 6 months sample indicates that large nano-particles started to dominate the PL process instead of small QDs. Even though showing weak excitation-dependent property, the sample still exhibit PL signals enduring 6 months exposure to the ambient conditions. This evidence the decent long-term stability of PtS_2's PL nature.

4. Conclusions

In summary, the fabrication of PtS_2 QDs suspension via a low-cost liquid exfoliation technique was demonstrated for the first time and the PL signals of PtS_2 QDs were clearly observed. The statistics of QDs illustrates an average dimension of 3.9 nm diameter with 2.9 nm thickness. The as-prepared PtS_2 QDs produce the maximum luminescent emission peak with a wavelength of 407.2 nm under the excitation wavelength of 328.5 nm. The excitation dependent luminescent property and size distribution of QDs confirm the quantum confinement effect. The great long-term stability of PtS_2 QDs may benefits prospective optics application. These findings indicate a promising future for luminescence applications.

Acknowledgements

This work is supported by Shenzhen Science and Technology Innovation Commission (JCYJ20170303160136888); National Natural Science Foundation of China (61575167); The Research Grants Council of Hong Kong, China (GRF 152109/16E PolyU B-Q52T).

References

[1] A.K. Geim, K.S. Novoselov, The rise of graphene, Nat. Mater. 6 (2007) 183. http://dx.doi.org/10.1038/nmat1849.

[2] X. Huang, Z. Zeng, H. Zhang, Metal dichalcogenide nanosheets: preparation, properties and applications, Chem. Soc. Rev. 42 (2013) 1934–1946. doi:10.1039/C2CS35387C.

[3] Q.H. Wang, K. Kalantar-Zadeh, A. Kis, J.N. Coleman, M.S. Strano, Electronics and optoelectronics of two-dimensional transition metal dichalcogenides, Nat. Nanotechnol. 7 (2012) 699. http://dx.doi.org/10.1038/nnano.2012.193.

[4] C. Tan, H. Zhang, Two-dimensional transition metal dichalcogenide nanosheet-based composites, Chem. Soc. Rev. 44 (2015) 2713–2731. doi:10.1039/C4CS00182F.

[5] J.N. Coleman, M. Lotya, A. O'Neill, S.D. Bergin, P.J. King, U. Khan, K. Young, A. Gaucher, S. De, R.J. Smith, I. V. Shvets, S.K. Arora, G. Stanton, H.-Y. Kim, K. Lee, G.T. Kim, G.S. Duesberg, T. Hallam, J.J. Boland, J.J. Wang, J.F. Donegan, J.C. Grunlan, G. Moriarty, A. Shmeliov, R.J. Nicholls, J.M. Perkins, E.M. Grieveson, K. Theuwissen, D.W. McComb, P.D. Nellist, V. Nicolosi, Two-Dimensional Nanosheets Produced by Liquid Exfoliation of Layered Materials, Science. 331 (2011) 568–571. doi:10.1126/science.1194975.

[6] L. Lin, Y. Xu, S. Zhang, I.M. Ross, A.C.M. Ong, D.A. Allwood, Fabrication of Luminescent Monolayered Tungsten Dichalcogenides Quantum Dots with Giant Spin-Valley Coupling, ACS Nano. 7 (2013) 8214–8223. doi:10.1021/nn403682r.

[7] S.Y. Lim, W. Shen, Z. Gao, Carbon quantum dots and their applications, Chem. Soc. Rev. 44 (2015) 362–381. doi:10.1039/C4CS00269E.

[8] S. Xu, D. Li, P. Wu, One‐Pot, Facile, and Versatile Synthesis of Monolayer MoS_2/WS_2 Quantum Dots as Bioimaging Probes and Efficient Electrocatalysts for Hydrogen Evolution Reaction, Adv. Funct. Mater. 25 (2015) 1127–1136. doi:10.1002/adfm.201403863.

[9] Z.X. Gan, L.Z. Liu, H.Y. Wu, Y.L. Hao, Y. Shan, X.L. Wu, P.K. Chu, Quantum confinement effects across two-dimensional planes in MoS_2 quantum dots, Appl. Phys. Lett. 106 (2015) 233113. doi:10.1063/1.4922551.

[10] H. Long, L. Tao, C.Y. Tang, B. Zhou, Y. Zhao, L. Zeng, S.F. Yu, S.P. Lau, Y. Chai, Y.H. Tsang, Tuning nonlinear optical absorption properties of WS_2 nanosheets, Nanoscale. 7 (2015) 17771–17777. doi:10.1039/C5NR04389A.

[11] H. Long, L. Tao, C.P. Chiu, C.Y. Tang, K.H. Fung, Y. Chai, Y.H. Tsang, The WS_2 quantum dot: preparation, characterization and its optical limiting effect in polymethylmethacrylate, Nanotechnology. 27 (2016) 414005. http://stacks.iop.org/0957-4484/27/i=41/a=414005.

[12] H. Li, X. He, Z. Kang, H. Huang, Y. Liu, J. Liu, S. Lian, C.H.A. Tsang, X. Yang, S. Lee, Water-Soluble Fluorescent Carbon Quantum Dots and Photocatalyst Design, Angew. Chemie Int. Ed. 49 (2010) 4430–4434. doi:10.1002/anie.200906154.

[13] S. Cao, C. Chen, J. Zhang, C. Zhang, W. Yu, B. Liang, Y. Tsang, MnO_x quantum dots decorated reduced graphene oxide/TiO_2 nanohybrids for enhanced activity by a UV pre-catalytic microwave method, Appl. Catal. B Environ. 176–177 (2015) 500–512. doi:https://doi.org/10.1016/j.apcatb.2015.04.041.

[14] P. V Kamat, Quantum Dot Solar Cells. Semiconductor Nanocrystals as Light Harvesters, J. Phys. Chem. C. 112 (2008) 18737–18753. doi:10.1021/jp806791s.

[15] L. Cao, X. Wang, M.J. Meziani, F. Lu, H. Wang, P.G. Luo, Y. Lin, B.A. Harruff, L.M. Veca, D. Murray, S.-Y. Xie, Y.-P. Sun, Carbon Dots for Multiphoton Bioimaging, J. Am. Chem. Soc. 129 (2007) 11318–11319. doi:10.1021/ja073527l.

[16] L. Li, W. Wang, Y. Chai, H. Li, M. Tian, T. Zhai, Few-Layered PtS_2 Phototransistor on h-BN with High Gain, Adv. Funct. Mater. 27 (2017) 1701011. doi:10.1002/adfm.201701011.

[17] Y. Zhao, J. Qiao, P. Yu, Z. Hu, Z. Lin, S.P. Lau, Z. Liu, W. Ji, Y. Chai, Extraordinarily Strong Interlayer Interaction in 2D Layered PtS_2, Adv. Mater. 28 (2016) 2399–2407. doi:10.1002/adma.201504572.

[18] P. Miró, M. Ghorbani-Asl, T. Heine, Two Dimensional Materials Beyond MoS_2: Noble-Transition-Metal Dichalcogenides, Angew. Chemie Int. Ed. 53 (2014) 3015–3018. doi:10.1002/anie.201309280.

[19] V. Tran, R. Soklaski, Y. Liang, L. Yang, Layer-controlled band gap and anisotropic excitons in few-layer black phosphorus, Phys. Rev. B. 89 (2014) 235319. doi:10.1103/PhysRevB.89.235319.

[20] X. Wang, P.K. Cheng, C.Y. Tang, H. Long, H. Yuan, L. Zeng, S. Ma, W. Qarony, Y.H. Tsang, Laser Q-switching with PtS_2 microflakes saturable absorber, Opt. Express. 26 (2018) 13055–13060. doi:10.1364/OE.26.013055.

[21] X. Chia, A. Adriano, P. Lazar, Z. Sofer, J. Luxa, M. Pumera, Layered Platinum Dichalcogenides (PtS_2, $PtSe_2$, and $PtTe_2$) Electrocatalysis: Monotonic Dependence on the Chalcogen Size, Adv. Funct. Mater. 26 (2016) 4306–4318. doi:10.1002/adfm.201505402.

[22] Y. Zhao, J. Qiao, Z. Yu, P. Yu, K. Xu, S.P. Lau, W. Zhou, Z. Liu, X. Wang, W. Ji, Y. Chai, High-Electron-Mobility and Air-Stable 2D Layered $PtSe_2$ FETs, Adv. Mater. 29 (2016) 1604230. doi:10.1002/adma.201604230.

[23] Y. Wang, L. Li, W. Yao, S. Song, J.T. Sun, J. Pan, X. Ren, C. Li, E. Okunishi, Y.-Q. Wang, others, Monolayer $PtSe_2$, a New Semiconducting Transition-Metal-Dichalcogenide, Epitaxially Grown by Direct Selenization of Pt, Nano Lett. 15 (2015) 4013–4018.

[24] K.S. Suslick, N.C. Eddingsaas, D.J. Flannigan, S.D. Hopkins, H. Xu, Extreme conditions during multibubble cavitation: Sonoluminescence as a spectroscopic probe, Ultrason. Sonochem. 18 (2011) 842–846. doi:10.1016/j.ultsonch.2010.12.012.

[25] V. Štengl, J. Henych, Strongly luminescent monolayered MoS_2 prepared by effective ultrasound exfoliation, Nanoscale. 5 (2013) 3387–3394.

[26] A.A. Audi, P.M.A. Sherwood, X-ray photoelectron spectroscopic studies of sulfates and bisulfates interpreted by X α and band structure calculations, Surf. Interface Anal. 29 (2000) 265–275. doi:10.1002/(SICI)1096-9918(200004)29:4<265::AID-SIA739>3.0.CO;2-3.

[27] X. Li, H. Wang, Y. Shimizu, A. Pyatenko, K. Kawaguchi, N. Koshizaki, Preparation of carbon quantum dots with tunable photoluminescence by rapid laser passivation in ordinary organic solvents, Chem. Commun. 47 (2011) 932–934. doi:10.1039/C0CC03552A.

[28] M. Hassan, E. Haque, K.R. Reddy, A.I. Minett, J. Chen, V.G. Gomes, Edge-enriched graphene quantum dots for enhanced photo-luminescence and supercapacitance, Nanoscale. 6 (2014) 11988–11994. doi:10.1039/C4NR02365J.

[29] X.L. Wu, J.Y. Fan, T. Qiu, X. Yang, G.G. Siu, P.K. Chu, Experimental Evidence for the Quantum Confinement Effect in 3C-SiC Nanocrystallites, Phys. Rev. Lett. 94 (2005) 26102. doi:10.1103/PhysRevLett.94.026102.

[30] A.M. Smith, S. Nie, Chemical analysis and cellular imaging with quantum dots, Analyst. 129 (2004) 672–677. doi:10.1039/B404498N.

[31] Y.-Y. Wang, X. Xiang, R. Yan, Y. Liu, F.-L. Jiang, Förster Resonance Energy Transfer from Quantum Dots to Rhodamine B As Mediated by a Cationic Surfactant: A Thermodynamic Perspective, J. Phys. Chem. C. 122 (2018) 1148–1157. doi:10.1021/acs.jpcc.7b08236.

[32] G.E. LeCroy, F. Messina, A. Sciortino, C.E. Bunker, P. Wang, K.A.S. Fernando, Y.-P. Sun, Characteristic Excitation Wavelength Dependence of Fluorescence Emissions in Carbon "Quantum" Dots, J. Phys. Chem. C. 121 (2017) 28180–28186. doi:10.1021/acs.jpcc.7b10129.

[33] S.H. Jin, D.H. Kim, G.H. Jun, S.H. Hong, S. Jeon, Tuning the Photoluminescence of Graphene Quantum Dots through the Charge Transfer Effect of Functional Groups, ACS Nano. 7 (2013) 1239–1245. doi:10.1021/nn304675g.

[34] W. Sukkabot, Stokes shift and fine structure splitting in composition-tunable ZnxCd1−xSe nanocrystals: Atomistic tight-binding theory, Phys. B Condens. Matter. 506 (2017) 192–197. doi:https://doi.org/10.1016/j.physb.2016.11.023.

[35] J. Pérez-Conde, A.K. Bhattacharjee, M. Chamarro, P. Lavallard, V.D. Petrikov, A.A. Lipovskii, Photoluminescence Stokes shift and exciton fine structure in CdTe nanocrystals, Phys. Rev. B. 64 (2001) 113303. doi:10.1103/PhysRevB.64.113303.

[36] Introduction to Fluorescence. In: Lakowicz J.R. (Eds.) Principles of Fluorescence Spectroscopy. Springer, Boston, MA, 2006, pp. 35-36.

[37] D.C. Turner, L. Brand, Quantitative Estimation, 7 (1968). doi:10.1021/bi00850a011.

Figure captions:

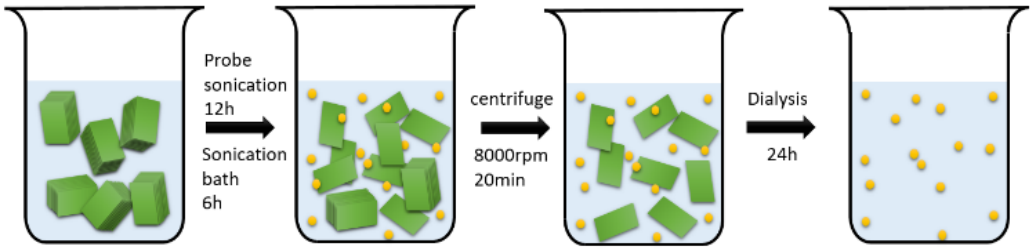

Fig. 1. Schematic representation of the synthesis process of PtS_2 QDs

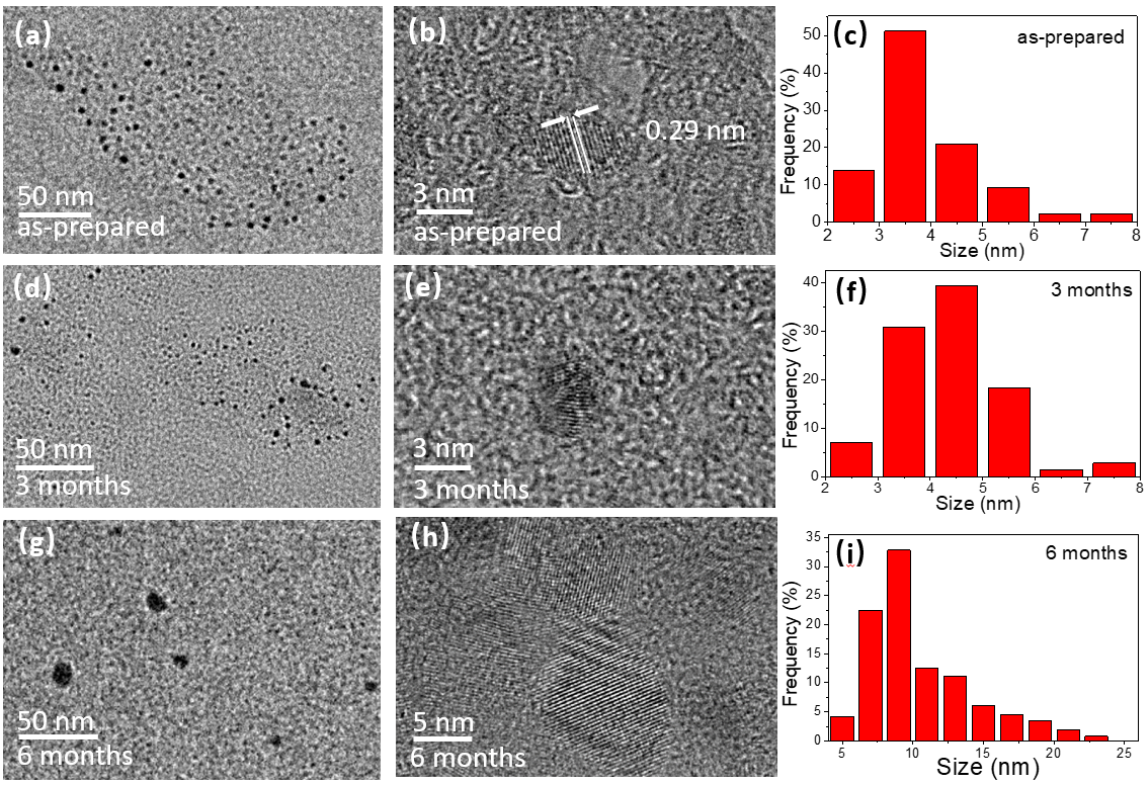

Fig. 2. (a) TEM image of as-prepared PtS_2 solution; (b) High-resolution TEM image of a typical QD in (a); (c) Size distribution of PtS_2 QDs in (a); (d) TEM image of PtS_2 solution stored for 3 months; (e) High-resolution TEM image of a typical QD in (d); (f) Size distribution of PtS_2 QDs in (d); (g) TEM image of PtS_2 solution stored for 6 months; (h) High-resolution TEM image of a typical nanoparticle in (g); (i) Size distribution of PtS_2 nanoparticles in (g).

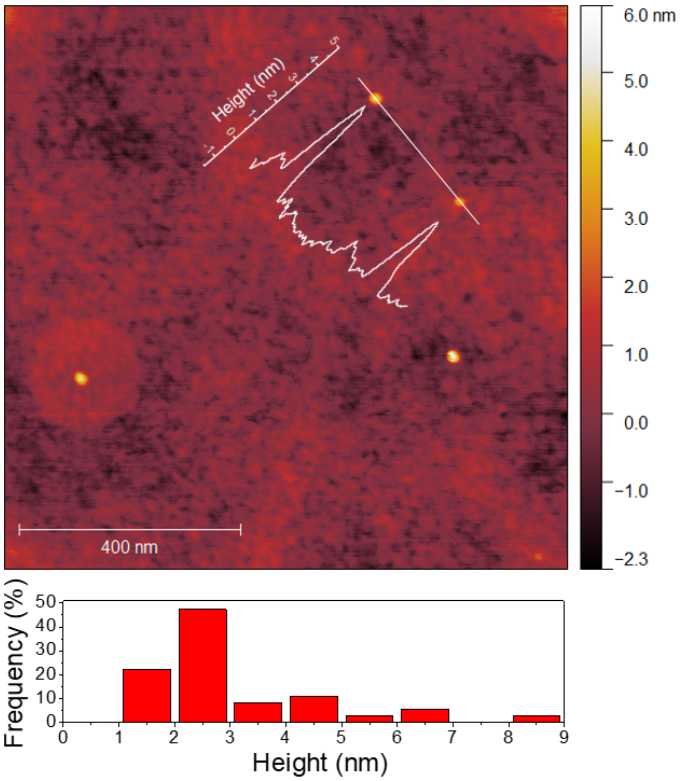

Fig. 3. AFM image of as-prepared PtS_2 QDs, the height profile along the straight lines (inset), and the statics of height distribution

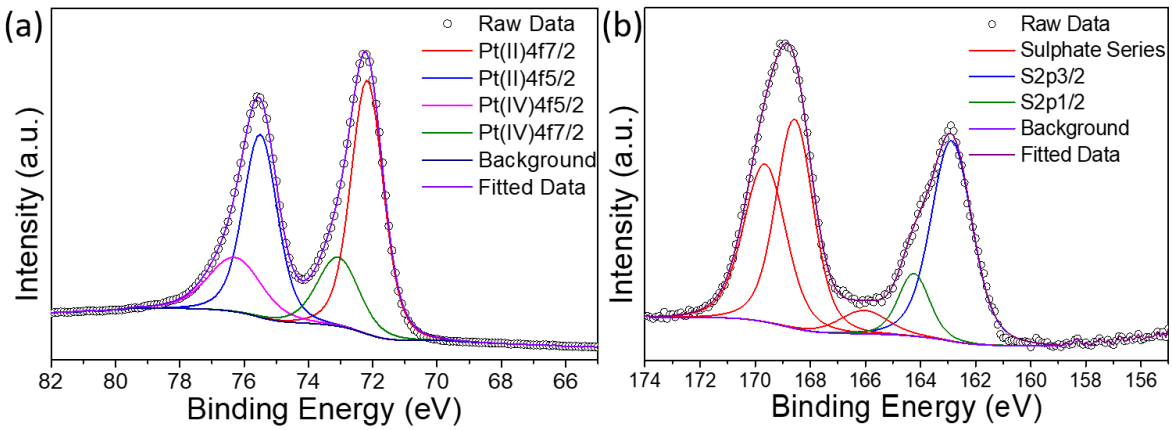

Fig. 4. High resolution X-ray photoelectron spectra of PtS_2 for (a) Pt4f region and (b) S2p region

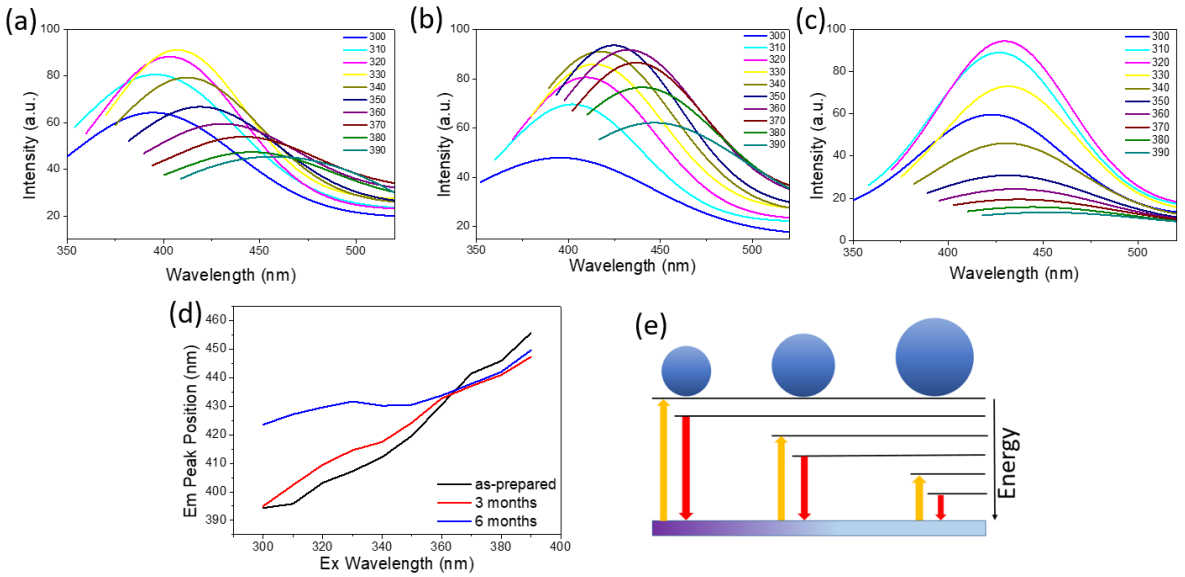

Fig. 5. (a) emission spectra of as-prepared solution; (b) emission spectra of solution stored for 3 months; (c) emission spectra of solution stored for 6 months; (d) Emission peak positions according to the excitation wavelengths; (e) Diagram of quantum size effect

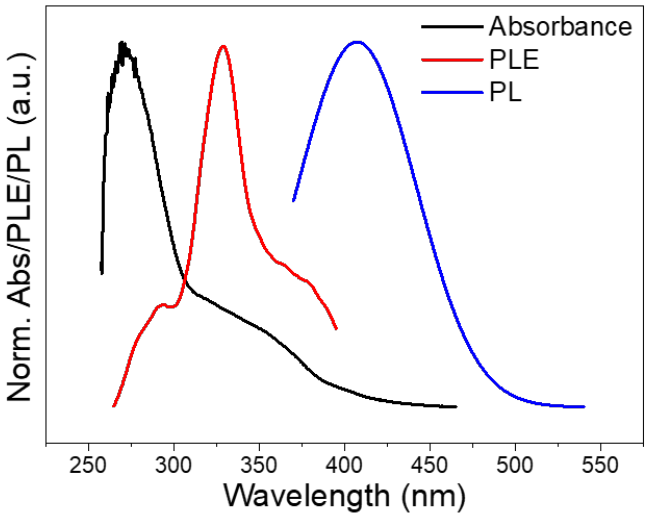

Fig. 6. Normalized Absorbance spectrum (black curve), Photoluminescence excitation spectrum (red curve), and Photoluminescence spectrum (blue curve) for the highest emission peak occurring at 407.21 nm of as-prepared sample